Two-Pass Robust Component Analysis for Cloud Removal in Satellite Image Sequence

Fei Wen, Yongjun Zhang, Zhi Gao, and Xiao Ling

***Abstract*— Due to the inevitable existence of clouds and their shadows in optical remote sensing images, certain ground-cover information is degraded or even appears to be missing, which limits analysis and utilization. Thus, cloud removal is of great importance to facilitate downstream applications. Motivated by the sparse representation techniques which have obtained a stunning performance in a variety of applications, including target detection, anomaly detection, and so on; we propose a two-pass robust principal component analysis (RPCA) framework for cloud removal in the satellite image sequence. First, a plain RPCA is applied for initial cloud region detection, followed by a straightforward morphological operation to ensure that the cloud region is completely detected. Subsequently, a discriminative RPCA algorithm is proposed to assign aggressive penalizing weights to the detected cloud pixels to facilitate cloud removal and scene restoration. Significantly superior to currently available methods, neither a cloud-free reference image nor a specific algorithm of cloud detection is required in our method. Experiments on both simulated and real images yield visually plausible and numerically verified results, demonstrating the effectiveness of our method.**

***Index Terms*— Clouds and shadows detection, image reconstruction, low rank, robust principal component analysis (RPCA).**

I. Introduction

DUE to the mechanism of optical sensors, satellite images are inevitably affected by cloud and accompanying shadow. As an example reported in [1], the Enhanced Thematic Mapper Plus land scenes are, on average, about 35% cloud covered globally. Cloud degrades or even completely occludes ground information in such remote sensing images, which remarkably limits the following analysis and utilization. Therefore, numerous studies have been concentrated on cloud removal so as to facilitate downstream applications of such remote sensing images.

According to the auxiliary information being leveraged on, the available cloud removal methods can be roughly grouped into three categories [2]: inpainting-based, multispectral-based, and multitemporal-based. Inpainting-based methods synthesize the cloud-contaminated region through propagating from neighboring noncloud pixels without any auxiliary data [3], [4]. However, such methods are fairly sensitive to the size of cloud, as the uncertainty and the error accumulate along with propagation. In the second category, leveraging on the properties of multispectral image, those cloud-free bands of the same multispectral image are exploited to estimate a linear or nonlinear relationship between cloudy band and cloud-free band(s). Subsequently, the estimated relationship is applied to recover the cloud-occupied region [5], [6]. However, such multispectral-based approaches usually can only deal with thin cloud, because thick cloud can exist in all bands of the multispectral image with a high possibility.

More relevant to this letter, the third category based on the aid of multitemporal images is more popularly investigated and applied. More specifically, the multitemporal information can be utilized either explicitly or implicitly, depending on whether the relationship between multitemporal images is explicitly exploited or implicitly formulated. In the former manner, [7] replaced the pixels occupied by clouds and accompanying shadows with the data of the same location from other cloud-free images. To eliminate seam effect, the replacement was implemented via color matching and multiscale wavelet-based fusion. In [2], the cloud-free patches were cloned to their corresponding cloud-contaminated patches under the assumption that land covers change slightly over a short time period. By solving a group of constrained Poisson equations, information clone yields visually consistent results. To further exploit the correlations between cloudy regions in the target image and cloud-free regions in both target and reference images, [8] improved a neighborhood similar pixel interpolator approach [9] to predict the cloud-contaminated pixels by combining spectral–spatial and spectral–temporal information. Reference [10] formulated a linear least-square regression model to search similar pixels and applied a spatially weighted regression for the reconstruction of cloud-contaminated pixels. In [11], the Markov random field model was applied to guide the replacement between similar pixels. Along the implicit manner, learning-based methods perform more elegantly to realize cloud removal. Reference [12] assumed that pixels in the cloudy area can be expressed as a linear combination of pixels in the cloud-free area, which was formulated and solved using sparse representation techniques. Reference [13] performed dictionary learning on target data and reference data separately in the spectral domain. Then, cloud removal was conducted by combining coefficients from the reference image and the dictionary learned from

Manuscript received January 16, 2018; revised March 8, 2018 and March 25, 2018; accepted April 17, 2018. Date of publication May 7, 2018; date of current version June 22, 2018. This work was supported in part by the National Key R&D Program of China under Grant 2017YFB0503004 and in part by the National Natural Science Foundation of China under Grant 41571434 and Grant 41322010. *(Corresponding author: Yongjun Zhang; Zhi Gao.)*

F. Wen, Y. Zhang, and X. Ling are with the School of Remote Sensing and Information Engineering, Wuhan University, Wuhan 430079, China (e-mail: wenfei@whu.edu.cn; zhangyj@whu.edu.cn; zyl_whu@163.com).

Z. Gao is with Temasek Laboratories, National University of Singapore, Singapore 117411 (e-mail: gaozhinus@gmail.com).

Color versions of one or more of the figures in this letter are available online at http://ieeexplore.ieee.org.

Digital Object Identifier 10.1109/LGRS.2018.2829028

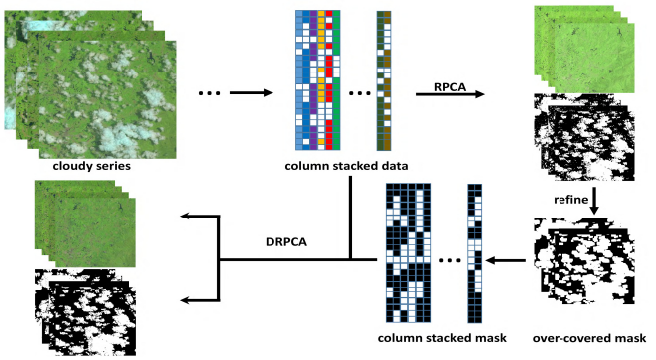

Fig. 1. Overview of the proposed two-pass RPCA method.

the target image. However, the reconstruction quality was sensitive to land-cover type and cloud size. Utilizing the local temporal correlations and the nonlocal spatial correlations, [14] introduced a patch-matching-based multitemporal group sparse representation (PM-MTGSR) method to recover cloud regions. In short, the available multitemporal-based methods have twofold disadvantages. First, extensive cloud-free reference images should be carefully chosen in advance. Second, a specific cloud detection method is required to locate the cloudy regions in the target images.

To overcome aforementioned disadvantages, we propose a two-pass robust principal component analysis (RPCA) framework for cloud removal in the satellite image sequence. First, the contiguous region of cloud is roughly and overly detected via a plain RPCA, followed by a straightforward morphological operation. Subsequently, a discriminative RPCA (DRPCA) which assigns aggressive penalizing weights to the detected cloud pixels is designed to facilitate cloud removal and scene restoration as well. Experiments on both simulated and real images yield visually plausible and numerically verified results, demonstrating the effectiveness of our method.

II. Methodology

Fig. 1 shows an overview of the major steps of our method.

A. Plain RPCA for Cloud and Shadow Detection

The RPCA [15] has obtained a stunning performance in a variety of applications, including target detection, anomaly detection, and so on. Suppose that the given data are arranged as the columns of a large matrix $M \in R^{m\times n}$, the RPCA can decompose M into a low-rank matrix L and a sparse matrix S, which is mathematically estimated by minimizing the following constrained convex optimization problem:

$$\min_{L,S} \|L\|_* + \lambda\|S\|_1 \quad \text{s.t. } M = L + S \tag{1}$$

where $\|L\|_*$ denotes the nuclear norm of matrix L, the sum of its singular value, and $\|S\|_1$ denotes the sum of the absolute value of matrix S, and λ is a positive balance value. Equation (1) can be treated as a general constrained convex optimization problem and solved by the inexact augmented Lagrange multiplier (ALM) method [16].

Benefiting from the revisit of remote sensing sensors, it is easy to obtain remote sensing image sequence of the same area. Given a sequence of aligned cloud-contaminated images (i.e., each image in the sequence is possibly contaminated by cloud), denoted as $I\{I_1, I_2, \ldots, I_n\}$, our purpose is to segment background land-cover and foreground cloud and its shadow from I. Regardless of slight land-cover changes, the cloud-free remote sensing images are linear correlated with each other for only considering illumination change, which can be perfectly modeled via a low-rank representation. Clouds and shadows, on the other hand, are sparse due to the transient nature of clouds, which are modeled as sparse outliers.

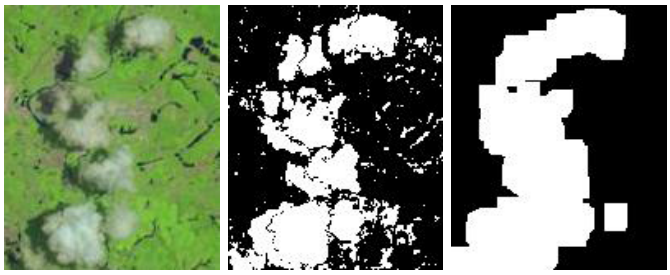

Fig. 2. Cloud and shadow mask. (Left) Original image block. (Middle) Binary segmentation. (Right) Morphological filtered mask.

Let matrix $D \in R^{m\times n}$ denote the column-stacked image sequence, $m = \text{rows} \times \text{cols}$ is the number of pixels in a single image, and n is the total number of images. By performing the RPCA on matrix D and unstacking the column format results, we obtain a sequence of cloud-free images and a sequence of outliers images from the low-rank component and the sparse component, respectively. Though a cloud-free sequence is generated at this step, it is not an ideal reconstruction result which we will discuss in Section II-B.

At last, we set a recommended threshold value to obtain the mask of clouds and their shadows in each image. However, the initial mask usually exhibits numerous noises, as shown in Fig. 2. Herein, the time interval between consecutive images ranges from a half month to several months, so that slight land-cover changes are screened out by thresholding. Fortunately, the size of most of land-cover changes is much smaller than clouds, according to which we can filter off most of noise and land-cover changes. The morphological filter is fairly simple yet good enough to refine binary masks to properly overcover the clouds and their shadows. We apply one morphological erode operator followed by three morphological dilate operators with the size of 3 in all our experiments.

B. DRPCA for Cloud Removal

All experiments in the first step apply the recommended value of $\lambda = 1/(\max(m,n))^{1/2}$ (where $m \times n$ are the dimensions of matrix D) in [16], and it works properly to screen out all the clouds and shadows. However, the low-rank component obtained in the original RPCA is too smooth (or blurred) for the reason that it is computed by iterative singular value decomposition (SVD) to reduce dimension, and a lot of unique information of each column is decomposed into sparse components. If we increase λ to generate a low-rank component with a higher rank to maintain an original cloud-free region, then more ghosts of cloud and its shadow will be left in the backgrounds indicating ineffective cloud and

shadow removal. As we find in our experiments, no single λ can simultaneously screen out all the clouds and their shadows and reconstruct a cloud-free sequence of which original cloud-free regions are maintained.

Inspired by the block sparse RPCA for salient motion detection in videos [17], pixels should be treated discriminatively according to their likelihood to be cloud pixels or cloud-free pixels. We set different balance values for cloud and shadow pixels and cloud-free pixels guided by the mask obtained in the first step, which we call it the DRPCA. Within an overcovered cloud mask, a lower balance value would ensure that all the cloud and its shadow will be entirely decomposed into an outlier matrix and not leave any ghostly presence in the background, yet without incurring a large false positive rate. For a cloud-free region, the balance value is set to a relatively large value to guarantee background maintenance. The new formulation is defined as

$$\min_{L,S} \|L\|_* + \alpha\|P_{\Omega}(S)\|_1 + \beta\|P_{\Omega^-}(S)\|_1 \quad \text{s.t. } D = L + S \tag{2}$$

where Ω is a clouds and shadows mask obtained in the first step, and Ω^- denotes a cloud-free region.

Equation (2) remains a constrained convex optimization problem, and an inexact ALM can still be applied to solve it. The augmented Lagrangian function is defined as

$$f(L, S, Y, \mu) = \|L|\|_* + \alpha\|P_{\Omega}(S)\|_1 + \beta\|P_{\Omega^-}(S)\|_1 + \langle Y, D - L - S\rangle + \frac{\mu}{2}\|D - L - S\|_F^2 \tag{3}$$

where $\|\cdot\|_F$ denotes the Frobenius norm, Y is the Lagrange multiplier, and μ is a positive scalar. Here, we present the algorithm based on an inexact ALM in Algorithm 1. For more details, readers can refer to [16].

Algorithm 1 Discriminated RPCA via Inexact ALM

Input: Matrix $D \in R^{m\times n}$, α, β and cloud mask Ω;
Output: low-rank L, sparse S;

$Y_0 = D/\ J(D)$; $S_0 = 0$; $\mu_0 > 0$; $\rho > 1$; $k = 0$.
while *not converged* **do**
  // Lines 4-5 solve $L_{k+1} = \arg\min_L\ f(L, S_k, Y_k, \mu_k)$
  $(U, \Lambda, V) = svd(D - S_k + \mu_k^{-1}Y_k)$;
  $L_{k+1} = US_{\mu_k^{-1}}[\Lambda]V^T$;
  // Line 7 solves $S_{k+1} = \arg\min_S f(L_{k+1}, S, Y_k, \mu_k)$;
  $S_{k+1} = (S_{\Omega_{\alpha\mu_k^{-1}}} + S_{\Omega^-\beta\mu_k^{-1}})[D - L + \mu_k^{-1}Y_k]$;
  $Y_{k+1} = Y_k + \mu_k(D - L_{k+1} - S_{k+1})$;
  $\mu_{k+1} = \rho\mu_k$;
  $k \leftarrow k + 1$;
end
Output L,S.

For the discriminated RPCA, the soft-thresholding operators $S_{\Omega}[\cdot]$ and $S_{\Omega^-}[\cdot]$ denote the shrinkage in Ω and Ω^-. The balance values α and β are set to $0.1/(\max(m, n))^{1/2}$ and 1, respectively. Except that, we use the recommended values and conditions in [16]. Specifically, we set $\mu_0 = 1.25/\|D\|_2$, $\rho = 1.6$, and $J(D) = \max(\|D\|_2, \alpha^{-1}\|D\|_\infty)$.

III. Experiments and Discussion

A. Test on Simulated Sequence

In order to quantitatively evaluate the performance of our method, we simulated three time series sequence of cloudy images based on cloud-free blocks cropped from Landsat-8 Operational Land Imager (OLI) scenes. All the Landsat-8 OLI scenes used in our experiments are Landsat-8 natural-look products which are compressed and stretched to create an optimization to images selection and visual interpretation. The LandsatLook Nature Color Image is composed of three bands (bands 4–6) and the reflectance values are scaled to 1–255 range using a gamma stretch and with a gamma value of 2. The stretch is designed to emphasize vegetation without clipping the extreme values. Images in the simulated sequence were well registered and listed according to their imaging time. For the reason that clouds and shadows are too complicate to simulate, we simply manually drew clouds in each image with pure white shapes and ignored the effect of cloud shadows. To evaluate the information reconstruction accuracy and efficiency of our method, two representative approaches, the Poisson information clone (PIC) in [2] and the PM-MTGSR in [14], were selected for comparison. The assessment of cloud and shadow detection performance would be discussed in a real images test. As shown in Fig. 3, most simulated images in the sequence are contaminated by cloud.

To simplify the reference image selection of the PIC and the PM-MTGSR, we manually chose the best suitable images for their reconstruction. All three methods were conducted in a single channel, and the reconstruction result is shown in Fig. 3. The three cloud removal approaches all yield visually plausible reconstruction and exhibit no obvious discontinuity around cloud mask boundaries. Compared with original cloud-free images, our reconstruction results show a slightly better consistency with original images than the PIC and PM-MTGSR methods as can be seen in the region marked by red rectangles in Fig. 3. This indicates that low rank is more powerful to maintain consistency in a whole image than the other two reconstruction methods. To quantitatively evaluate the three reconstruction methods, the root-mean-square error, the peak signal-to-noise ratio, and the structural similarity index are used to assess their reconstruction accuracy. Table I shows that the proposed DRPCA reconstructs the cloudy images better than the other two methods.

Finally, an efficiency comparison about processing images with a different cloud cover-rate is also presented. We simulated a larger size of cloud on the same image in Fig. 3(a). The DRPCA processes a sequence of images one time so that the time of reconstructing a single image is divided by the total number of images. As shown in Table II, the reconstruction time of the PIC method increases dramatically with cloud coverage-rate getting larger. The kernel step of solving the Poisson equation with the boundary condition is to solve a large system of linear equations, which is time-consuming when cloud size is getting larger. The PM-MTGSR method spends too much time for reconstruction due to dictionary learning and sparse coding. On the other hand,

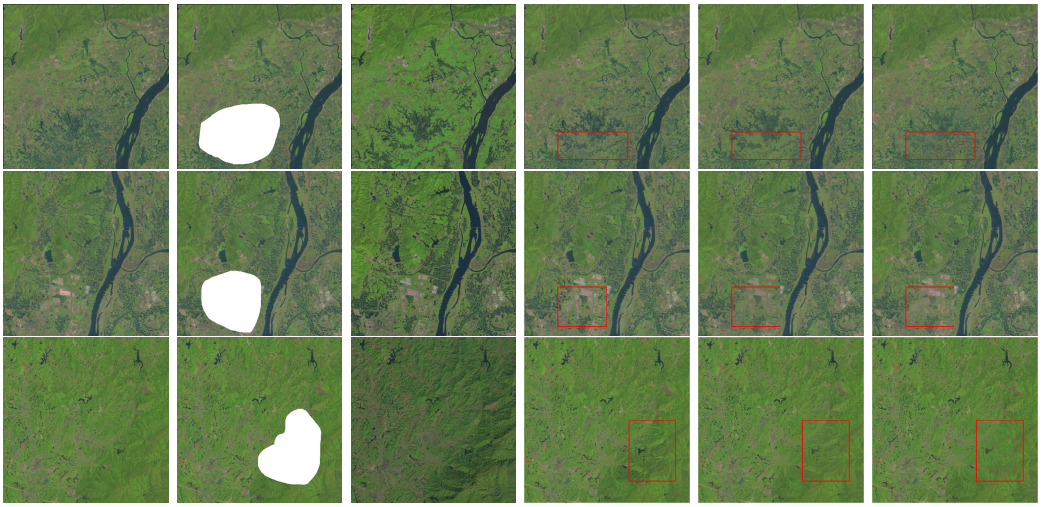

Fig. 3. Three cloud removal examples of simulated data. (a) Original cloud-free images prepared for simulation. (b) Simulated cloudy images. (c) Selected cloud-free image with significant atmospheric difference, which is displayed for comparison. (d)–(f) Cloud removal results by PIC, PM-MTGSR, and our method, respectively.

TABLE I

QUANTITATIVE ASSESSMENT OF DIFFERENT METHODS. IMAGES 1–3 ARE THREE EXAMPLES IN FIG. 3(b). SIMULATION AND CLOUD-FREE DENOTE SIMULATED CLOUD IMAGE AND CLOUD-FREE IMAGE FOR COMPARISON, RESPECTIVELY. THE BEST EVALUATION VALUES BETWEEN THE THREE METHODS ARE HIGHLIGHTED

Image	Method	RMSE	PSNR	SSIM
Image1	simulation	5.9857	12.3824	0.8695
	cloud-free	2.2700	22.1149	0.8317
	PIC	2.8835	34.1911	0.9689
	PM-MTGSR	2.7730	31.4813	0.9660
	DRPCA	**2.4614**	**36.9887**	**0.9792**
Image2	simulation	5.2695	14.2536	0.8987
	cloud-free	2.9051	23.9133	0.8588
	PIC	2.2535	35.8949	0.9832
	PM-MTGSR	**1.2620**	36.3862	0.9871
	DRPCA	1.8150	**38.1807**	**0.9877**
Image3	simulation	5.5039	12.8524	0.8811
	cloud-free	1.6691	21.6349	0.8641
	PIC	**1.5776**	39.0756	0.9953
	PM-MTGSR	1.8786	**40.7129**	0.9967
	DRPCA	1.8925	40.6417	**0.9971**

TABLE II

EFFICIENCY COMPARISON BETWEEN PIC, PM-MTGSR, AND THE PROPOSED DRPCA

Image	Cloud percentage	PIC(s)	PM-MTGSR(s)	DRPCA(s)
Image1	20.33%	83.07	1279.4	1.18
	25.00%	117.35	1364.1	1.23
Image2	10.95%	34.81	1165.8	1.18
	30.53%	160.82	1388.0	1.23
Image3	10.75%	34.13	1201.3	1.18
	24.97%	112.92	1255.4	1.23

the DRPCA iteratively decomposes the input matrix into a low-rank component and a sparse component through one SVD in each iteration. We find in our experiments that the DRPCA converges less than 15 iterations when dealing with a sequence of about 30 images. More importantly, the time of the PIC for processing a single image is larger than that of the DRPCA for processing a whole sequence of images. In summary, the DRPCA can reconstruct a cloudy remote sensing image sequence with a high accuracy and efficiency.

B. Test on Real Images

We used three real sequence data sets containing a heterogeneous land-cover type to test the robustness and effectiveness of the proposed approach. Each real sequence consisted of about 30 cloudy images with different cloud contamination levels. Differed from traditional studies that assumed completely cloud-free reference images, our cloud-cover rate ranged from 1% to 52%, which was more practical in real world. We set threshold value for detecting clouds and shadows as the standard value of sparse component S, and a clouds and shadows mask was generated by thresholding on the absolute value of S. Fig. 4 shows the cloud removal results of the proposed method. Our approach can recover visually plausible cloud-free images even though images are severely covered by clouds and shadows. At the meantime, the clouds and shadows detection results are of high quality as shown in Fig. 5. Our final binary mask was generated by combining three masks which were obtained in three single channels. As studied in [18] and [19], clouds and shadows detection is another area of research dedicated in detecting all kinds of cloud. Though we did not compare our detection results with those well-studied methods quantitatively, which can be one of our future works, the generated clouds and shadows mask shows a high accuracy visually. However, obvious false detections occurred on a large area of sudden changes as shown in red regions of Fig. 5. This is because such changes belong to a single image in the sequence and no similar features exist in the remaining images, so it is screened out as outlier just like clouds and shadows. Such cases may happen when the image sequence corresponds to a very long temporal interval. That is to say, our method may prone to sudden large area land-cover changes.

IV. CONCLUSION AND FUTURE WORK

In this letter, we propose a two-pass RPCA framework for cloud removal in the satellite image sequence. Significantly superior to the available methods, neither cloud-free reference

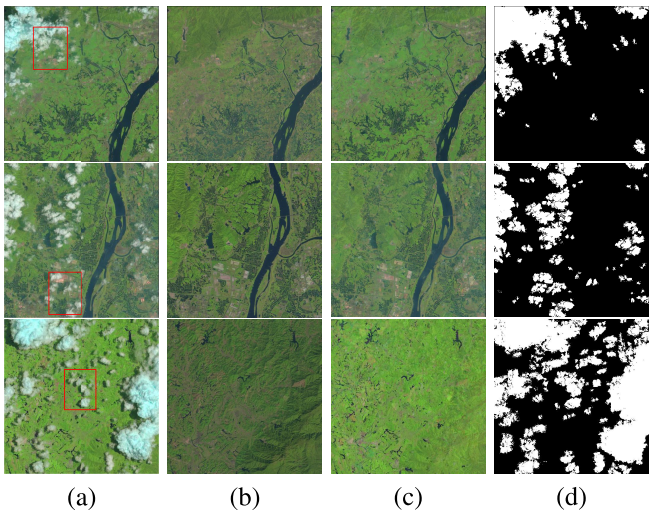

Fig. 4. Experiments on real data. (a) Real cloudy images. (b) Cloud-free image with significant atmospheric difference, which is selected for comparison. (c) Reconstructed results of our method. (d) Cloud and shadow detection results.

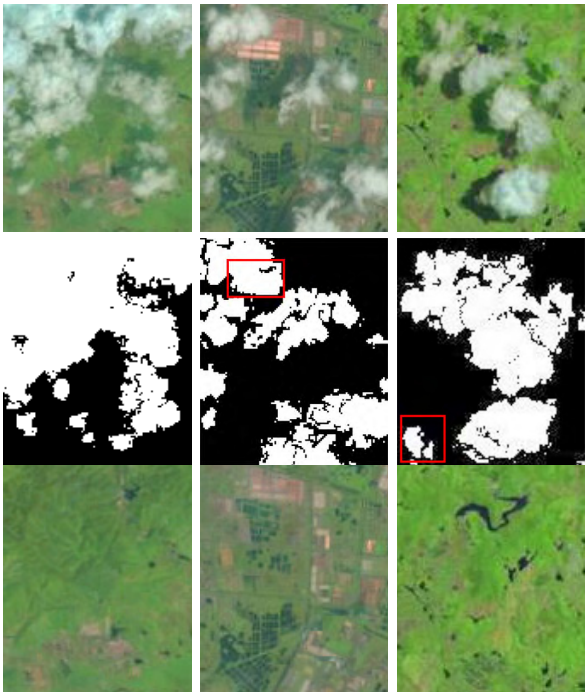

Fig. 5. Clouds and shadows detection results in zoomed-in view of the block in Fig. 4. The second row is zoomed cloud and shadow masks. The third row is zoomed recovered results.

images nor a specific algorithm of cloud detection is required in our method. Experiments demonstrate that the proposed method could recover the cloudy images more precisely than state-of-the-art methods. More importantly, our method exhibits a tremendous efficiency improvement compared with those methods. On the other hand, our method generated high quality clouds and shadows detection results as a by-product, which combined the two traditional works (i.e., clouds and shadows detection and image reconstruction) into a whole, showing a great potential to be applied for possessing a remote sensing image sequence. In addition, there is still room for improvement. In particular, the shadow on the lower cloud casted by those higher cloud may have similar appearance to the real land-covers, which makes the problem more subtle to formulate and solve. Furthermore, we are working on distinguishing outliers of land-cover changes from that of cloud and shadow to improve robustness. Thus, more insightful context information, either spatial or temporal, or both, should be incorporated for more robust cloud removal solution.

REFERENCES

[1] J. Ju and D. P. Roy, "The availability of cloud-free landsat ETM + data over the conterminous United States and globally," *Remote Sens. Environ.*, vol. 112, no. 3, pp. 1196–1211, 2008.

[2] C.-H. Lin, P.-H. Tsai, K.-H. Lai, and J.-Y. Chen, "Cloud removal from multitemporal satellite images using information cloning," *IEEE Trans. Geosci. Remote Sens.*, vol. 51, no. 1, pp. 232–241, Jan. 2013.

[3] A. Maalouf, P. Carré, B. Augereau, and C. Fernandez-Maloigne, "A bandelet-based inpainting technique for clouds removal from remotely sensed images," *IEEE Trans. Geosci. Remote Sens.*, vol. 47, no. 7, pp. 2363–2371, Jul. 2009.

[4] L. Lorenzi, F. Melgani, and G. Mercier, "Inpainting strategies for reconstruction of missing data in VHR images," *IEEE Geosci. Remote Sens. Lett.*, vol. 8, no. 5, pp. 914–918, Sep. 2011.

[5] M. Xu, X. Jia, and M. Pickering, "Automatic cloud removal for Landsat 8 OLI images using cirrus band," in *Proc. IEEE Int. Geosci. Remote Sens. Symp. (IGARSS)*, Jul. 2014, pp. 2511–2514.

[6] P. Rakwatin, W. Takeuchi, and Y. Yasuoka, "Restoration of Aqua MODIS band 6 using histogram matching and local least squares fitting," *IEEE Trans. Geosci. Remote Sens.*, vol. 47, no. 2, pp. 613–627, Feb. 2009.

[7] D.-C. Tseng, H.-T. Tseng, and C.-L. Chien, "Automatic cloud removal from multi-temporal SPOT images," *Appl. Math. Comput.*, vol. 205, no. 2, pp. 584–600, 2008.

[8] X. Zhu, F. Gao, D. Liu, and J. Chen, "A modified neighborhood similar pixel interpolator approach for removing thick clouds in Landsat images," *IEEE Geosci. Remote Sens. Lett.*, vol. 9, no. 3, pp. 521–525, May 2012.

[9] J. Chen, X. Zhu, J. E. Vogelmann, F. Gao, and S. Jin, "A simple and effective method for filling gaps in Landsat ETM + SLC-off images," *Remote Sens. Environ.*, vol. 115, no. 4, pp. 1053–1064, 2011.

[10] B. Chen, B. Huang, L. Chen, and B. Xu, "Spatially and temporally weighted regression: A novel method to produce continuous cloud-free Landsat imagery," *IEEE Trans. Geosci. Remote Sens.*, vol. 55, no. 1, pp. 27–37, Jan. 2017.

[11] Q. Cheng, H. Shen, L. Zhang, Q. Yuan, and C. Zeng, "Cloud removal for remotely sensed images by similar pixel replacement guided with a spatio-temporal MRF model," *ISPRS J. Photogramm. Remote Sens.*, vol. 92, pp. 54–68, Jun. 2014.

[12] L. Lorenzi, F. Melgani, and G. Mercier, "Missing-area reconstruction in multispectral images under a compressive sensing perspective," *IEEE Trans. Geosci. Remote Sens.*, vol. 51, no. 7, pp. 3998–4008, Jul. 2013.

[13] M. Xu, X. Jia, M. Pickering, and A. J. Plaza, "Cloud removal based on sparse representation via multitemporal dictionary learning," *IEEE Trans. Geosci. Remote Sens.*, vol. 54, no. 5, pp. 2998–3006, May 2016.

[14] X. Li, H. Shen, H. Li, and L. Zhang, "Patch matching-based multitemporal group sparse representation for the missing information reconstruction of remote-sensing images," *IEEE J. Sel. Topics Appl. Earth Observ. Remote Sens.*, vol. 9, no. 8, pp. 3629–3641, Mar. 2016.

[15] E. J. Candès, X. Li, Y. Ma, and J. Wright, "Robust principal component analysis?" *J. ACM*, vol. 58, no. 3, p. 11, May 2011.

[16] Z. Lin, M. Chen, and Y. Ma. (2010). "The augmented Lagrange multiplier method for exact recovery of corrupted low-rank matrices." [Online]. Available: https://arxiv.org/abs/1009.5055

[17] Z. Gao, L.-F. Cheong, and Y.-X. Wang, "Block-sparse RPCA for salient motion detection," *IEEE Trans. Pattern Anal. Mach. Intell.*, vol. 36, no. 10, pp. 1975–1987, Oct. 2014.

[18] Z. Li, H. Shen, H. Li, G. Xia, P. Gamba, and L. Zhang, "Multi-feature combined cloud and cloud shadow detection in GaoFen-1 wide field of view imagery," *Remote Sens. Environ.*, vol. 191, pp. 342–358, Mar. 2017.

[19] S. Qiu, B. He, Z. Zhu, Z. Liao, and X. Quan, "Improving Fmask cloud and cloud shadow detection in mountainous area for Landsats 4–8 images," *Remote Sens. Environ.*, vol. 199, pp. 107–119, Sep. 2017.